Second Harmonic Excitation Spectroscopy of Silver Nanoparticle Arrays

Andrew M. Moran, Jiha Sung, Erin M. Hicks, Richard P. Van Duyne, and Kenneth G. Spears*

Chemistry Department, Northwestern University, Evanston, Illinois 60208-3113

Received: July 21, 2004; In Final Form: November 30, 2004

Frequency-scanned excitation profiles of coherent second harmonic generation (SHG) were measured for silver nanoparticle arrays prepared by nanosphere lithography. The frequency of the fundamental beam did not coincide with the localized surface plasmon resonance (LSPR) of the nanoparticles and was tuned so that the coherent second harmonic (SH) emission was in the region of the LSPR at 720−750 nm. The SH emission from the arrays was compared with a smooth silver film to identify an enhancement of SH emission efficiency that peaks near ∼650 nm for nanoparticles 50 nm in height. The polarization and orientation dependence of this enhancement suggests that it is related to a dipolar LSPR mode polarized normal to the plane of the substrate. Linear extinction spectra are dominated by in-plane dipoles and do not show this weak out-of-plane LSPR mode. The nanoparticle arrays are truncated tetrahedrons symmetrically oriented by nanosphere lithography to cancel SH from in-plane dipoles which allows observation of the weak out-of-plane component.

I. Introduction

Current interest in the optical properties of nanoscale materials is driven by a broad spectrum of technological applications, including bio/chemosensors,[1,2] optical filters,[3] plasmonic waveguides,[4−9] and substrates for surface-enhanced molecular spectroscopy.[10−12] Noble metal nanoparticles are particularly well-suited for these applications because of their size, shape, and environment sensitive localized surface plasmon resonance (LSPR) bands. Current fabrication methods allow the LSPR energies and the widths of individual particles[13−17] and ordered arrays[18−21] to be tuned with high precision. Many applications use the linear optical response of the LSPR modes. Fundamental studies of nonlinear optical properties represent a relatively new method of studying nanoparticle properties.

In this work, we characterize linear and nonlinear optical properties of silver nanoparticle arrays fabricated by nanosphere lithography.[18,19,22−24] The extinction spectra and second harmonic generation (SHG) are measured for various orientations and polarizations, and the coherent SHG is studied with a tunable femtosecond laser. The fundamental beam is not resonant with the material, whereas the emitted frequency is tuned in the region of the LSPR to identify resonance behavior. The SHG from a silver film is measured to compare with the array SHG at every wavelength to allow experimental parameter normalization.

Experimental studies of second-order optical properties for metal nanoparticles were reported for colloids dispersed in solution,[25−29] embedded in a dielectric matrix,[30−32] and supported on a substrate.[33−40] These investigations include measurements of both hyper-Rayleigh scattering (HRS)[25−28] and coherent SHG.[30−40] Hupp and co-workers[25] reported the first experimental distinction between electric dipole and quadrupole contributions to HRS for solutions of spherical 32 nm silver nanoparticles by comparing angularly resolved emission with predictions from a theoretical model. In addition, nanoparticle-enhanced SHG was recently studied for a fluorescent polymer adsorbed on 100 nm gold particles.[41]

Several theoretical studies were reported for particles with simple geometric shapes.[33,42−49] Specific treatments include a hydrodynamic model for an electron gas,[43] a quantum size effect formulation for conduction electrons,[44] and an extension of the continuous dipolium model[50] to a sphere in an inhomogeneous longitudinal field.[51] Most predictions for complex shapes are made by assuming an intensity independent nonlinear response which is expressed as the product of linear susceptibilities.[52] A general formalism for arbitrarily shaped particles in inhomogeneous dielectric environments is not yet available. The second harmonic (SH) signals from silver films are consistent with the general form of the second-order susceptibility and a tight-binding basis set.[53−55] The SH signals from the nanoparticle arrays are analyzed by considering general multipolar interaction mechanisms.

Methods for sample preparation and spectroscopic characterization are outlined in the following section. Results and discussion are presented in section III, and in section IV, we provide a conclusion and an outlook for further studies

II. Experimental Methods

II.A. Sample Preparation. *Materials.* Silver (99.99%) was purchased from D. F. Goldsmith (Evanston, IL). The glass substrates were no. 2 coverslips, 18 mm in diameter, from Fisher Scientific (Fairlawn, VA). Pretreatment of the glass substrates required H_2SO_4, H_2O_2, and NH_4OH, which were obtained from Fisher Scientific. Surfactant-free white carboxyl-substituted polystyrene latex nanospheres 390 nm in diameter were received as a suspension in water from Duke Scientific (Palo Alto, CA); the 510 nm nanospheres were purchased from Interfacial Dynamics (Portland, OR). Absolute ethanol was purchased from Pharmco (Brookfield, CT).

Substrates. Glass substrates were cleaned by immersion in a boiling piranha solution (3:1 concentrated H_2SO_4/30% H_2O_2) for 30 min. After cooling, the substrates were thoroughly rinsed with Millipore water until the solution reached a pH of 5. The substrates were then sonicated for 1 h in 5:1:1 $H_2O/NH_4OH/$

10.1021/jp0467604 CCC: $30.25
Published on Web 02/12/2005

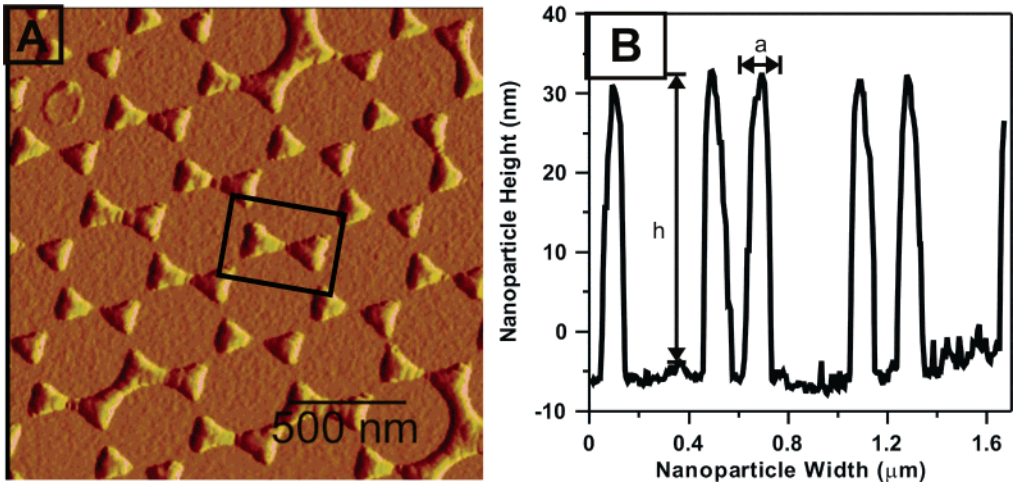

Figure 1. (A) AFM image of a sample prepared with a nanosphere diameter of 390 nm. The perpendicular bisector, *a*, of the triangular base is 100 nm, and the interparticle distance is 294 nm. The box depicts the centrosymmetry of particle pairs present in the sample. (B) A line scan of the sample in (A) verifies the theoretical calculations with $a = 104$ nm and a height = 52 nm.

30% H_2O_2. Following sonication, the substrates were rinsed with Millipore water until the solution reached a pH of 5, and then they were stored in Millipore water until used.

Nanoparticle Arrays and Silver Films. Single-layer nanoparticle arrays were prepared with the nanosphere lithography technique.[19,22,24] A suspension of nanospheres spontaneously self-assembled into hexagonally close-packed two-dimensional arrays after being coated on a clean glass substrate. Once the sphere masks were dry, half of the mask was removed with tape and a razor blade to leave an area of bare glass where the film would be deposited. Silver was deposited at a rate of 0.1 nm s^{-1} with a Consolidated Vacuum Corp. (Rochester, NY) deposition system. The deposited height was monitored with a XTM/2 monitor quartz crystal microbalance (Leybold Inficon, East Syracuse, NY).

The number of deposition steps depended on the height of the particle array. The desired particle height (25−50 nm) was achieved during the first deposition. If necessary, the height of the Ag film was increased to 50 nm during a second deposition to ensure that a continuous smooth film with minimal islands and roughness features was present. The nanoparticle portion of the cover slip was masked with Al foil during the second deposition. On the day of the optical measurements, the nanosphere masks were removed by sonication in absolute ethanol for approximately 5 min.

Atomic Force Microscopy (AFM). AFM images were collected with a Digital Instruments Nanoscope III microscope operated in tapping mode with etched Si nanoprobe tips (Digital Instruments, Santa Barbara, CA). These tips have resonance frequencies between 280 and 320 kHz, a conical shape with a cone angle of 20°, and an effective radius of curvature at the tip of 10 nm. Figure 1 shows an AFM image of a typical sample prepared with 390 nm nanospheres. This image and earlier studies by nanosphere lithography support the dimensional properties of each nanoparticle as a truncated tetrahedron.The triangular base of each tetrahedron has a perpendicular bisector of ∼90−100 nm, and the nanoparticles form hexagonal arrays around the 390 nm diameter of the nanosphere. The geometric relationships have been previously described[19,22,24] in terms of the nanosphere diameter, *D*. The triangular base has a perpendicular bisector *a* that equals 0.233*D*, and the interparticle center-to-center spacing, d_{ip}, equals 0.577*D* Figure 1 demonstrates that the pattern is composed of pairs of tetrahedra in the defect-free sections of the surface, which is important for discussing SHG properties. The particle arrays have a number of defects which have been described but not correlated with optical properties.[24,56] The sizes of the defect-free regions are unknown, but prior work suggests that they are probably small (∼10 μm) so, with a spot size of 125 μm in our experiments, we cannot assume uniform symmetry. An array prepared with 390 nm nanospheres with a height of 50 nm has an extinction maximum of 620−630 nm. For the array on glass, theoretical modeling suggests that the particle coupling is weak for particles with this spacing.[57]

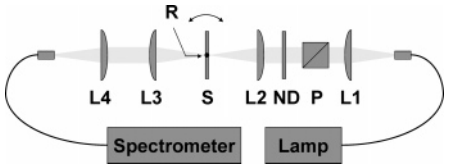

Figure 2. Experimental design used for extinction measurements. Symbols represent achromatic lenses (L1−L4), polarizer (P), neutral density filter (ND), sample (S), and a rotational axis for the sample (R).

II.B. Extinction Measurements. The optical design used to measure extinction is shown in Figure 2. A continuum (∼400−900 nm) generated by a tungsten−halogen source was focused to a spot size of 600 μm (fwhm) on the sample with an achromatic lens. A polarizer was used to control incident light polarization. Sample orientation (normal, 45°, and 70° incidence) was varied with a graduated rotational mount. Extinction spectra were collected with an optical-fiber-coupled Ocean Optics model USB2000 spectrometer. With a nominal height of 50 nm, the 390 and 510 nm sphere diameters gave extinctions peaking at 620−630 and 720−750 nm, respectively.

II.C. SHG Measurements. Experiments were carried out with an amplified Ti−Sapphire laser system described in a prior publication.[58] The output of the compressor is centered at 805 nm with a spectral bandwidth of 22 nm and a pulse duration of 90 fs at 1 kHz. A tunable near-IR fundamental beam was generated with a laboratory-built optical parametric amplifier (OPA) pumped by 650 μJ/pulse of the amplified Ti−Sapphire beam. The total near-IR output of the OPA was 50 μJ/pulse (signal + idler). A polarizer separated the signal and idler pulses. The duration and bandwidth of the signal pulse are 125 fs and 430 cm^{-1} (at 1.3 μm), respectively. Pulse energy was controlled with neutral density filters.

The SHG experimental configuration is shown in Figure 3. The fundamental was focused to 125 μm (∼100 000 particles)

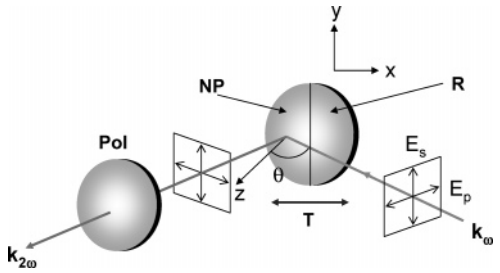

Figure 3. Configuration used for SHG measurements. A coordinate system is also defined. Symbols represent the incidence angle (q), Ag nanoparticle arrays (NP), Ag film reference (R), polarizer (Pol), and translation stage (T). We use polarization notation to refer to input/output polarization directions as s:s or p:p.

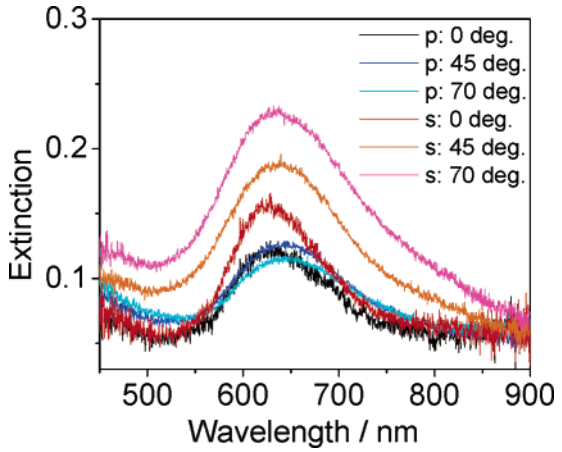

Figure 4. Polarization and orientation dependent extinction spectra. The magnitudes are approximate.

with a +20 cm focal length CaF_2 lens at incident angles of 10 and 45°. Polarization was varied with an achromatic (1000−1600 nm) $\lambda/2$ waveplate. The second harmonic was collected with a +10 cm focal length lens, and then passed through a thin film polarizer and a short-pass color filter (Schott KG-3 or Corning 1-69) before being focused into an Acton SpectroPro 2300i spectrometer. A liquid nitrogen-cooled Princeton Instruments SPEC-10 CCD: 400 (LN) camera was used for detection. We used apertures to prove that the output SHG signal was in a coherent beam.

Both p-polarized and s-polarized emissions were recorded while the fundamental beam was tuned from 1.16 to 1.52 μm. The fundamental beam was focused on four spots on the sample by translating the sample stage. The sample stage was oriented to translate parallel to the sample plane, so the detection alignment was equivalent for all positions on the sample. Two of the four spots were on the nanoparticle array, while the other two were on the smooth film. This procedure was designed to minimize changes in detection alignment between the nanoparticle array and the silver film reference.

III. Results and Discussion

III.A. Extinction Measurements. Polarization and orientation dependent extinction measurements are shown in Figure 4. Spectra recorded at normal, 45°, and 70° incidence are shown, but absolute magnitude comparisons are only approximate. The goal of these studies was to determine if any large changes in extinction could be found near 600−700 nm as the polarization and incidence angle were varied to enhance the perpendicular components of extinction. These data represent a typical result. However, each preparation leads to slightly different results in shape and peak location as a function of angle, and different spots in the same sample are not exactly identical. The angle tuning changes the sample area illuminated, so we expect some spectral variation as a function of angle and difficulty in identifying any but very large spectral changes. The spectra in Figure 4 show no large changes in the 600 nm region, which is of interest for interpreting the data shown below. Our equipment was not able to scan below 450 nm, and more complete spectra in this region were previously reported for these nanoparticle arrays. Theoretical studies of LSPR predict that dipolar and quadrupolar plasmon modes polarized both in and out of the plane of the substrate should exist for particles of this type, and these modes were used to assign features in the nanoparticle spectra.[17,59] The out-of-plane dipolar mode was not clearly identified experimentally, probably because of its much weaker extinction.[17] By analogy, we assign the dominant feature at 630 nm to an in-plane dipolar mode and the weak extinction peak in the 450 nm region to a quadrupole component. The general theoretical prediction for particles of our dimensions is that the out-of-plane dipolar resonance is to the blue of the in-plane dipolar absorption at ~700 nm, but red-shifted with respect to the in-plane quadrupole at ~400−450 nm. Theoretical models will require explicit inclusion of the substrate to more accurately predict relative intensities and wavelengths for all transitions.

III.B. Nanoparticle Annealing. Noble metal nanoparticles can be annealed with a high-power laser beam,[60,61] so measurements were made to ensure that the fluence used for studying SHG was not within this regime. A 300 μm pinhole was placed over a sample, and the extinction spectra were measured before and after irradiation with a near-IR beam (1300 nm). A fraction (45 or 65%) of the near-IR beam was allowed to pass through the pinhole. No change in the spectrum was observed at fluences below 4.4 mJ cm^{-2} which correspond to a power of 300 μW for our SHG experimental setup (beam spot size of 125 μm fwhm at the focus and 1 kHz repetition rate). However, the extinction peak blue shifted by ~20 nm after irradiation at a fluence of 7.00 mJ cm^{-2} corresponding to a power of 750 μW. We also directly tested SHG intensity versus incident power, and a logarithmic plot deviated from linearity after ~400 μW. Both results ensure that the sample is safe until 300 μW with a power threshold of about 400 μW. The power used for the SHG measurements (III.C and III.D) was 100−300 μW (pulse energy of 100−300 nJ), corresponding to a fluence of 1.46−4.37 mJ cm^{-2} through the central 25% of the focus spot.

III.C. SHG Excitation Spectra. We begin this section by briefly reviewing the resonance structure of the second-order response. The second-order susceptibility is most simply stated as a product of linear susceptibilities[62]

$$\chi^{(2)}_{ijj}(2\omega;\omega,\omega) = -\frac{mb}{N^2e^3}\chi^{(2)}_{ii}(2\omega)[\chi^{(1)}_{jj}(\omega)]^2 \qquad (1)$$

where m is the electron mass, b is a nonlinear coefficient, N is the plasma electron density, and e is a unit charge. The linear susceptibilities, $\chi^{(1)}_{jj}(\omega)$, are written in tensor form with indices ij that represent electric field polarizations and frequency arguments that represent the fundamental (ω) and emitted waves (2ω). The frequency dependence is easily predicted by inspection of eq 1. In the absence of centrosymmetric SHG cancellation, the resonance enhancement in our case should result from the $\chi^{(1)}_i(2\omega)$ factor since the fundamental frequency is far from any linear resonance; the SHG excitation profiles should exhibit maxima at the peak positions seen in the linear extinction spectra.

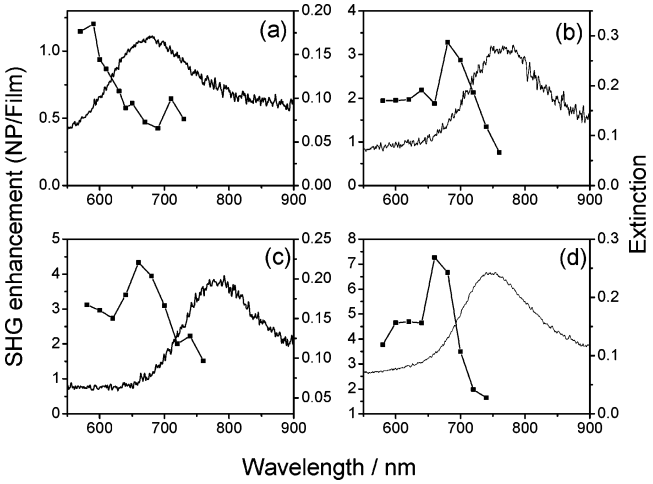

Figure 5. SHG enhancement for nanoparticle arrays (NP) divided by SHG from the Ag film (Film) (connected points) measured for (a and b) p-in/p-out at 45° incidence and (c and d) p-in/p-out at 10° incidence. The extinction spectrum (continuous curve) is shown for comparison. All profiles are on different samples.

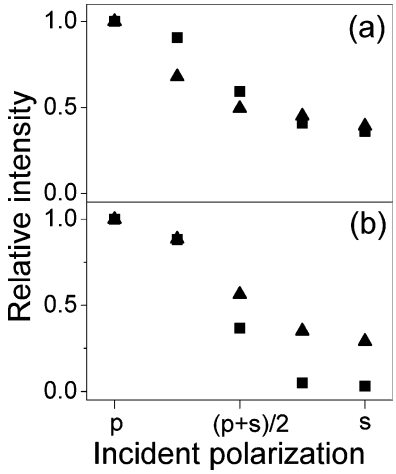

Figure 6. Normalized SHG intensity detected in p polarization at (a) 10 and (b) 45° incidence for both the nanoparticle arrays (triangles) and smooth film (squares).

A typical SHG excitation profile measured for p:p (fundamental/SH emission) polarization conditions at incidence angles of 10 and 45° is shown in Figure 5 for four different particle arrays. The enhancement factor is the ratio of the SH signal from the array divided by SH from the silver film and is not adjusted for the reduced particle area (∼7.2% of the film). Although alignment variations made accurate quantification difficult, we can conservatively state that the absolute signals (not shown) for 10° were 7−15 times weaker than those at 45°. The absolute integrated SH count for p:p polarization at 45° was ∼2000 counts/s.

A peak in the p:p SHG efficiency was found for all particle arrays with extinction maxima ranging from 650 to 800 nm; samples with this extinction range were chosen because of the tuning range of our laser system. The peak was blue-shifted with respect to the extinction peak by 80−120 nm depending on the sample. Particle arrays with extinction maxima near 600 nm were needed to probe the SHG efficiency to the red of the extinction maximum (laser tunes from 1.16 to 1.52 μm). However, no resonances were found for this case. The data for Figure 5 show that both 45 and 10° angles of incidence give similar SH profiles for the p:p experiment. There is greater opportunity at 10° than at 45° to excite in-plane dipole components, but the similar resonance behavior supports the hypothesis that this resonance is dominated by an out-of-plane transition. We observed the peak in SHG efficiency at ∼650−670 nm for arrays prepared with a height of ∼50 nm. There are features in Figure 5 that might be interpreted as substructure, but they are sample specific and may not be significant. The sample defects do not allow azimuthal rotation of the sample to probe pattern orientation effects in an unambiguous manner.

The p:p SH emission was ∼10 times more intense than the s:s emission. There was a sample dependent spectral response of the s:s signals. The usual case was a weak signal, but some samples showed weak signals with different profiles suggesting that these polarizations probe small differences in sample preparation.

A general consideration of SHG enhancement mechanisms provides physical insight for the present work. Three radiation−matter interactions occur for the second-order processes. Local interactions occur by electric dipole (E1) coupling, whereas the electric quadrupole (E2) and magnetic dipole (M1) modes are the leading nonlocal contributions. All possible permutations of the interaction mechanisms are allowed for a noncentrosymmetric array of particles. However, electric dipole terms should dominate the response, so as a first approximation, paths that involve more than one nonlocal interaction are neglected leaving a total of five distinguishable mechanisms for SHG. These five mechanisms can be represented as E1 + E1 → E1, E1 + E2 → E1, E1 + M1 → E1, E1 + E1 → E2, and E1 + E1 → M1. The E1 + E1 → E1 contribution should vanish when a sufficient number of randomly oriented particles are illuminated or for arrays made with centrosymmetric orientation.[37]

The truncated tetrahedral particles shown in Figure 1 comprise a lattice[24] in which centrosymmetry of in-plane dipoles should result in cancellation of SHG when a sufficient number of particles are contained within the spot of the laser beam. The array can be considered to be made of particle pairs that have inversion symmetry, whereas individual particles do not have inversion symmetry. The symmetric character of the array, therefore, suppresses resonance enhancement from the in-plane dipolar mode, and no peak in the SHG efficiency is observed at the 780 nm extinction maximum in Figure 5. We might expect the E1 + E2 → E1 (E1 + E1 → E2) mechanism to contribute if the input (output) frequencies are in resonance with quadrupolar modes. However, theoretical calculations[59] place the in-plane quadrupole at 400−450 nm for particles of these dimensions, so we did not assign the observed SHG enhancement to a quadrupole resonance. The polarization, orientation, and frequency dependence of the SHG enhancement is consistent with a weak out-of-plane dipolar resonance, which contributes through the E1 + E1 → E1 mechanism. This resonance is theoretically predicted to absorb weakly at the approximate frequency of the observed peak, so we tentatively assigned the SHG enhancement to an out-of-plane dipolar mode. The position of this resonance should be sensitive to particle height and size, and therefore, variations of these parameters will be required to test this conclusion.

III.D. Polarization Dependent SHG. Polarized measurements made at a fixed input frequency were used to compare the tensorial response of the films to the nanoparticle arrays. Silver films ∼50 nm in height were studied with no resonances at either the fundamental or SH frequencies. Typical polarization and orientation dependent results for both a film and an array are presented in Figure 6. The wavelength of the fundamental beam was 1300 nm, and the peak extinction for this array was 650 nm; however, similar results were found with the same fundamental beam and a LSPR frequency of 750 nm. The input

polarization of the fundamental was varied from p to s with p-polarized SH detection. Results for s-polarized emission are too weak for peak integration, particularly in the case of the film. SHG from the silver film is highly sensitive to the out-of-plane electric field component of the fundamental beam, which is most easily seen for larger angles of incidence when the difference between p and s is most significant. In Figure 6, we see that at 45° the film shows a sharp decrease in p-polarized output when the input polarization varies from p to s, whereas at 10°, the trend is the same but the variation is less severe. In contrast, SHG from the array is less sensitive to variation of the incidence angle and input polarization with the effect being most obvious at 45°.

The data can be interpreted with a model that was successfully applied to the magneto-optical Kerr effect.[53−55] This model provides a qualitative picture in which tensor elements are considered in terms of in-plane and out-of-plane matrix elements. We first write the *i*-polarized component SHG intensity as the square of the second-order polarization

$$I_i(2\omega;\omega) \approx |\vec{P}_i^{(2)}(2\omega)|^2 \tag{2}$$

The polarization, $\vec{P}_i^{(2)}(2\omega)$, can be expressed in terms of the second-order susceptibility tensor, $\chi_{ijl}^{(2)}(2\omega;\omega)$, and the fundamental local electric fields, $\vec{E}_j(2\omega)\vec{E}_k^{(2)}(\omega)$, as

$$\vec{P}_i^{(2)}(2\omega) = \chi_{ijl}^{(2)}(2\omega;\omega)\vec{E}_j(2\omega)\vec{E}_k(\omega) \tag{3}$$

The second-order susceptibility is written in a discrete basis truncated to include only conducting electrons[55]

$$\chi_{ijl}^{(2)}(2\omega;\omega) = \sum_{abc\in\text{cond,band}} \langle a|\hat{e}_i|b\rangle\langle b|\hat{e}_j|c\rangle\langle c|\hat{e}_k|a\rangle F_{abc}(\omega,2\omega) \tag{4}$$

where $F_{abc}(\omega,2\omega)$ contains transmission and reflection coefficients as well as all energetic parameters and $\hat{e}_i$ is an electric field component. Restriction of the sum over states to the conduction band is valid when the fundamental frequency is less than the difference between the Fermi energy and the d-band (∼4 eV for silver). Predictions are intuitive on tight binding of atomic orbitals. The following rules may be applied to matrix elements for the film (coordinate system of Figure 3):

$$\langle a|\hat{e}_z|b\rangle \neq 0 \text{ and } \langle a|\hat{e}_x|b\rangle = \langle a|\hat{e}_y|b\rangle = 0 \tag{5}$$

These rules hold for all crystalline faces of silver and for an amorphous surface.

The dominance of out-of-plane emission for the film is consistent with predictions of the model, and this result is general for smooth noble metal surfaces. Results for the nanoparticle array reveal the sensitivity of SHG to the properties of individual particles even when the SHG is not resonant. The excitation profiles discussed in the previous section showed that the SHG resonance enhancement is related to an out-of-plane component, but Figure 6 suggests that the absolute emission intensity for the nanoparticle array possesses significant in-plane contributions as well. The rules outlined in eq 5 cannot be applied to the array because of its finite nanoparticle height and spatial extent, a conclusion supported by these polarization measurements. This type of data would be especially useful for testing theoretical models when the orientations of individual particles have simpler symmetry and are uniform over the focus area. Our nanoparticle arrays have more complicated symmetry and include defects that prevent azimuthal studies.

IV. Conclusion

Frequency-scanned excitation profiles of coherent SHG were measured for silver nanoparticle arrays prepared by nanosphere lithography. The maxima in the p:p SHG efficiencies were blue-shifted by 80−120 nm from the peak of the in-plane dipolar LSPR. The location of the SHG peak is ∼670−690 nm for nanoparticle arrays with a height of ∼50 nm prepared from 510 nm nanospheres. The data were interpreted by assuming that the purely in-plane dipolar emission mechanism is suppressed because of averaging over a centrosymmetric distribution of nanoparticles. Polarization and orientation dependent measurements suggest that SHG is enhanced by a LSPR mode polarized out-of-plane, which was not observed in the linear spectrum because of its weak extinction. This is the first clear identification of such a resonance for shaped nanoparticles, and it was only possible because of the cancellation of in-plane dipolar emission. Unlike Ag films, measurements of single-wavelength and polarization-controlled SHG intensity from nanoparticle arrays when the SHG was not resonant showed a moderate in-plane component from the nanoparticle array where this is forbidden. The experimental identification of out-of-plane dipolar LSPR will provide a key test of theoretical models for nanoparticle optical properties. Future work will probe quadrupole resonances to provide a full test of the nanoparticle response theory for nonspherical nanoparticles.

Acknowledgment. This work was supported by the Air Force Office of Scientific Research MURI program (F49620-03-1-0381).

References and Notes

(1) Haes, A. J.; Van Duyne, R. P. *J. Am. Chem. Soc.* **2002**, *124*, 10596.
(2) Storhoff, J. J.; Elghanian, R.; Mucic, R. C.; Mirkin, C. A.; Letsinger, R. L. *J. Am. Chem. Soc.* **1998**, *120*, 1959.
(3) Dirix, Y.; Bastiaansen, C.; Caseri, W.; Smith, P. *Adv. Mater.* **1999**, *11*, 223.
(4) Knoll, W. *Annu. Rev. Phys. Chem.* **1998**, *49*, 569.
(5) Quinten, M.; Leitner, A.; Krenn, J. R.; Aussenegg, F. R. *Opt. Lett.* **1998**, *23*, 1331.
(6) Bozhevolnyi, S. I.; Erland, J.; Leosson, K.; Skovgaard, P. M. W.; Hvam, J. M. *Phys. Rev. Lett.* **2001**, *86*, 3008.
(7) Weeber, J. C.; Krenn, J. R.; Dereux, A.; Lamprecht, B.; Lacroute, Y.; Goudonnet, J. P. *Phys. Rev. B* **2001**, *64*, 045411.
(8) Brongersma, M. L.; Hartman, J. W.; Atwater, H. A. *Phys. Rev. B* **2000**, *62*, R16356.
(9) Egusa, S.; Liau, Y. H.; Scherer, N. F. *Appl. Phys. Lett.* **2004**, *84*, 1257.
(10) Freeman, R. G.; Grabar, K. C.; Allison, K. J.; Bright, R. M.; Davis, J. A.; Guthrie, A. P.; Hommer, M. B.; Jackson, M. A.; Smith, P. C.; Walter, D. G.; Natan, M. J. *Science* **1995**, *267*, 1629.
(11) Kahl, M.; Voges, E.; Kostrewa, S.; Viets, C.; Hill, W. *Sens. Actuators B* **1998**, *51*, 285.
(12) Haynes, C. L.; Van Duyne, R. P. *J. Phys. Chem. B* **2003**, *107*, 7426.
(13) Lee, S. M.; Jun, Y. W.; Cho, S. N.; Cheon, J. *J. Am. Chem. Soc.* **2002**, *124*, 11244.
(14) Petroski, J. M.; Green, T. C.; El-Sayed, M. A. *J. Phys. Chem. A* **2001**, *105*, 5542.
(15) Jana, N. R.; Gearheart, L.; Murphy, C. J. *J. Phys. Chem. B* **2001**, *105*, 4065.
(16) Kim, F.; Song, J. H.; Yang, P. *J. Am. Chem. Soc.* **2002**, *124*, 14316.
(17) Jin, R.; Cao, Y.; Mirkin, C. A.; Kelly, K. L.; Schatz, G. C. *J. Am. Chem. Soc.* **2002**, *124*, 15182.
(18) Hulteen, J. C.; Van Duyne, R. P. *J. Vac. Sci. Technol., A* **1995**, *13*, 1553.
(19) Hulteen, J. C.; Treichel, D. A.; Smith, M. T.; Duval, M. L.; Jensen, T. R.; Van Duyne, R. P. *J. Phys. Chem. B* **1999**, *103*, 3854.
(20) Walraff, G. M.; Hinsberg, W. D. *Chem. Rev.* **1999**, *99*, 1801.
(21) Ito, T.; Okazaki, S. *Nature* **2000**, *406*, 1027.

(22) Haynes, C. L.; Van Duyne, R. P. *J. Phys. Chem. B* **2001**, *105*, 2222.
(23) Haynes, C. L.; McFarland, A. D.; Smith, M. T.; Hulteen, J. C.; Van Duyne, R. P. *J. Phys. Chem. B* **2002**, *106*, 1898.
(24) Haynes, C. L.; Van Duyne, R. P. *J. Phys. Chem. B* **2001**, *105*, 5599.
(25) Hao, E. C.; Schatz, G. C.; Johnson, R. C.; Hupp, J. T. *J. Chem. Phys.* **2002**, *117*, 5963.
(26) Johnson, R. C.; Li, J. T.; Hupp, J. T.; Schatz, G. C. *Chem. Phys. Lett.* **2002**, *356*, 534.
(27) Santos, B. S.; Pereira, A. L.; Petrov, D. V.; de Mello Donegá, C. *Opt. Commun.* **2000**, *178*, 187.
(28) Jacobsohn, M.; Banin, U. *J. Phys. Chem. B* **2000**, *104*, 1.
(29) Bavli, R.; Yogev, D.; Efrima, S.; Berkovic, G. *J. Phys. Chem.* **1991**, *95*, 7422.
(30) Podlipensky, A.; Lange, J.; Seifert, G.; Graener, H.; Cravetchi, I. *Opt. Lett.* **2003**, *28*, 716.
(31) Sandrock, M. L.; Pibel, C. D.; Geiger, F. M.; Foss, C. A., Jr. *J. Phys. Chem. B* **1999**, *103*, 2668.
(32) Antoine, R.; Pellarin, M.; Palapant, B.; Broyer, M.; Prével, B.; Galleto, P.; Brevet, P. F.; Girault, H. H. *J. Appl. Phys.* **1998**, *84*, 4532.
(33) Chen, C. K.; Heinz, T. F.; Ricard, D.; Shen, Y. R. *Phys. Rev. B* **1983**, *27*, 1965.
(34) Götz, T.; Buck, M.; Dressler, C.; Eisert, F.; Träger, F. *Appl. Phys. A* **1995**, *60*, 607.
(35) Simon, M.; Trager, F.; Assion, A.; Lang, B.; Voll, S.; Gerber, G. *Chem. Phys. Lett.* **1998**, *296*, 579.
(36) Muller, T.; Vaccaro, P. H.; Balzer, F.; Rubahn, H. G. *Opt. Commun.* **1997**, *135*, 103.
(37) Lamprecht, B.; Leitner, A.; Aussenegg, F. R. *Appl. Phys. B* **1999**, *68*, 419.
(38) Srinivasan, R.; Tian, Y.; Suni, I. I. *Surf. Sci.* **2001**, *490*, 308.
(39) Tuovinen, H.; Kauranen, M.; Jefimovs, K.; Vahimaa, P.; Vallius, T.; Turunen, J.; Tkachenko, N. V.; Lemmetyinen, H. *J. Nonlinear Opt. Phys. Mater.* **2002**, *11*, 421.
(40) Hayakawa, T.; Usui, Y.; Bharathi, S.; Nogami, M. *Adv. Mater.* **2004**, *16*, 1408.
(41) Clark, H. A.; Campagnola, P. J.; Wuskell, J. P.; Lewis, A.; Loew, L. M. *J. Am. Chem. Soc.* **2000**, *122*, 10234.
(42) Bloembergen, N.; Chang, R. K.; Jha, S. S.; Lee, C. H. *Phys. Rev.* **1968**, *174*, 813.
(43) Hua, X. M.; Gersten, J. I. *Phys. Rev. B* **1986**, *33*, 3756.
(44) Lo, K. Y.; Lue, J. T. *Phys. Rev. B* **1995**, *51*, 2467.
(45) Dewitz, J. P.; Hübner, W.; Bennemann, K. H. *Z. Phys. D* **1996**, *28*, 169.
(46) Guerrero, A.; Mendoza, B. S.; Mochán, W. L. *Phys. Rev. B* **2000**, *62*, 11152.
(47) Zheludev, N. I.; Emel'yanov, V. I. *J. Opt. A: Pure Appl. Opt.* **2004**, *6*, 26.
(48) Dadap, J. I.; Shan, J.; Eisenthal, K. B.; Heinz, T. F. *Phys. Rev. Lett.* **1999**, *83*, 4045.
(49) Dadap, J. I.; Shan, J.; Heinz, T. F. *J. Opt. Soc. Am. B* **2004**, *21*, 1328.
(50) Mendoza, B. S.; Mochán, W. L. *Phys. Rev. B* **1996**, *53*, 4999.
(51) Brudny, V. L.; Mendoza, B. S.; Mochán, W. L. *Phys. Rev. B* **2000**, *62*, 11152.
(52) Schatz, G. C.; Van Duyne, R. P. Electromagnetic Mechanism of Surface-Enhanced Spectroscopy. In *Handbook of Vibrational Spectroscopy*; Chalmers, J. M., Griffiths, P. R., Eds.; Wiley: New York, 2002; p 759.
(53) Pustogowa, U.; Hübner, W.; Bennemann, K. H. *Phys. Rev. B* **1993**, *48*, 8607.
(54) Hübner, W. *Phys. Rev. B* **1990**, *42*, 11553.
(55) Hübner, W.; Bennemann, K. H.; Böhmer, K. *Phys. Rev. B* **1994**, *50*, 17597.
(56) Rossi, R. C.; Lewis, N. S. *J. Phys. Chem. B* **2001**, *105*, 12303.
(57) Jensen, T. R.; Schatz, G. C.; Van Duyne, R. P. *J. Phys. Chem. B* **1999**, *103*, 2394.
(58) Marin, T. W.; Homoelle, B. J.; Spears, K. G.; Hupp, J. T.; Spreer, L. O. *J. Phys. Chem. A* **2002**, *106*, 1131.
(59) Kelly, K. L.; Coronado, E.; Zhao, L. L.; Schatz, G. C. *J. Phys. Chem. B* **2003**, *107*, 668.
(60) Kawasaki, M.; Hori, M. *J. Phys. Chem. B* **2003**, *107*, 6760.
(61) Link, S.; Burda, C.; Mohamed, M. B.; Nikoobakht, B.; El-Sayed, M. A. *J. Phys. Chem. A* **1999**, *103*, 1165.
(62) Shen, Y. R. *The Principles of Nonlinear Optics*; Wiley: New York, 1984.